Multiscale Evaluation of the Improvements in Surface Snow Simulation through Terrain Adjustments to Radiation

SUJAY V. KUMAR

Science Applications International Corporation, Beltsville, and Hydrological Sciences Laboratory, NASA Goddard Space Flight Center, Greenbelt, Maryland

CHRISTA D. PETERS-LIDARD

Hydrological Sciences Laboratory, NASA Goddard Space Flight Center, Greenbelt, Maryland

DAVID MOCKO

Science Applications International Corporation, Beltsville, Global Modeling and Assimilation Office, and Hydrological Sciences Laboratory, NASA Goddard Space Flight Center, Greenbelt, Maryland

YUDONG TIAN

Earth System Science Interdisciplinary Center, College Park, and Hydrological Sciences Laboratory, NASA Goddard Space Flight Center, Greenbelt, Maryland

(Manuscript received 22 March 2012, in final form 25 September 2012)

ABSTRACT

The downwelling shortwave radiation on the earth's land surface is affected by the terrain characteristics of slope and aspect. These adjustments, in turn, impact the evolution of snow over such terrain. This article presents a multiscale evaluation of the impact of terrain-based adjustments to incident shortwave radiation on snow simulations over two midlatitude regions using two versions of the Noah land surface model (LSM). The evaluation is performed by comparing the snow cover simulations against the 500-m Moderate Resolution Imaging Spectroradiometer (MODIS) snow cover product. The model simulations are evaluated using categorical measures, such as the probability of detection of ''yes'' events (PODy), which measure the fraction of snow cover presence that was correctly simulated, and false alarm ratio (FAR), which measures the fraction of no-snow events that was incorrectly simulated. The results indicate that the terrain-based correction of radiation leads to systematic improvements in the snow cover estimates in both domains and in both LSM versions (with roughly 12% overall improvement in PODy and 5% improvement in FAR), with larger improvements observed during snow accumulation and melt periods. Increased contribution to PODy and FAR improvements is observed over the north- and south-facing slopes, when the overall improvements are stratified to the four cardinal aspect categories. A two-dimensional discrete Haar wavelet analysis for the two study areas indicates that the PODy improvements in snow cover estimation drop to below 10% at scales coarser than 16 km, whereas the FAR improvements are below 10% at scales coarser than 4 km.

1. Introduction

The importance of snow cover estimates for a variety of hydrologic and water resources applications is well recognized (Barnett et al. 2005). Through its high albedo and low thermal conductivity, snow cover exerts strong influences on land atmosphere energy exchanges and on the evolution of atmospheric conditions (Cohen and Entekhabi 1999). The seasonal and interannual variability of snow cover affects the seasonal freeze and thaw of the ground and the timing and duration of snowmelt processes. The snowmelt, in turn, impacts the soil moisture and runoff fields, which are important for several end-use applications such as water resources and agricultural management.

Spaceborne sensors have been employed since the 1960s to generate estimates of fractional snow cover

Corresponding author address: Sujay Kumar, Hydrological Sciences Laboratory, NASA GSFC, Code 617, Greenbelt, MD 20771. E-mail: sujay.v.kumar@nasa.gov

DOI: 10.1175/JHM-D-12-046.1

© 2013 American Meteorological Society

area (fSCA) and its distribution over continental and hemispheric scales. Visible and infrared sensors are typically used to provide measurements of fSCA at high spatial resolutions such as 250 m (Hall et al. 2002). These sensors, however, are limited to observing under cloud-free conditions, introducing significant gaps in the measurements (Ackerman et al. 1998). Furthermore, these retrievals are also subject to measurement noise and errors in retrieval models. Alternatively, land surface models (LSMs) and data assimilation systems are used to generate estimates of snow conditions. Though LSMs can be configured to simulate spatially and temporally continuous estimates of snow conditions at the desired resolutions, they also suffer from uncertainties in model inputs and in their representation of physical processes. For example, forcing inputs or the meteorological boundary conditions for the LSMs are typically available at coarse spatial resolutions as they are often prescribed from the outputs of global atmospheric models. As a result, these inputs must be appropriately downscaled to finer spatial and temporal resolutions before employing them for high-resolution snow model simulations.

Among different meteorological inputs to the LSMs, the incident radiation from the sun is the primary source of energy to the snowpack and is modified based on the slope and aspect of the land surface (Whiteman 2000). Several snow modeling studies have explored statistical relationships between snow estimates, meteorological variables, and topographic features (Evans et al. 1989; Elder et al. 1998; Winstral et al. 2002; Erickson et al. 2005). In the Northern Hemisphere, north-facing slopes receive less radiation from the sun during the winter relative to the south-facing slopes. Over the east- and west-facing slopes, the terrain influences on the amount of incident radiation are mostly diurnal adjustments. For example, the east-facing slopes receive radiation from the sun in the morning when the air temperatures are colder, while the west-facing slopes receive sunshine in the afternoon when the air temperatures are warmer. These local terrain effects significantly impact the evolution of snow over terrain slopes. These topographic effects on solar input are generally included only in distributed models at fine spatial scales (Dozier 1979; Tarboton et al. 1995; Cline 1997; Luce et al. 1998; Liston et al. 1999; Liston and Elder 2006; Helbig and Löwe 2012).

In a recent study, Barlage et al. (2010) examined the effects of terrain-based adjustments to solar radiation inputs using Noah LSM. This study was focused on evaluating the modeled snow water equivalent (SWE) estimates from Noah LSM against in situ and the Snow Data Assimilation System (SNODAS) analysis products from the National Operational Hydrologic Remote Sensing Center (NOHRSC). In their comparisons conducted over a domain in Colorado at 2-km spatial resolution, the improvements from terrain corrections were found to be small. Here we extend this analysis to the evaluation of snow cover estimates by comparing against a satellite-based product at 1-km spatial resolution.

Large land surface modeling efforts such as the Global Land Data Assimilation System (GLDAS; Rodell et al. 2004) and the North American Land Data Assimilation System (NLDAS; Mitchell et al. 2004) run model simulations at coarser scales, 25 km globally and 12.5 km over the continental United States, respectively. Similarly, land data assimilation systems used in operations at the National Centers for Environmental Prediction (NCEP; Saha et al. 2010) and at the Air Force Weather Agency (AFWA) run global land analyses at approximately 38-km and 25-km resolution, respectively. Furthermore, these operational centers also run regional domain simulations at various spatial resolutions (1–25 km) to initialize the weather forecast models. For these different applications, it is beneficial to quantify how the impacts of terrain effects on incident shortwave radiation and the corresponding improvements in snow simulations translate to the relevant spatial scale. This study provides a multiscale evaluation of the topographic correction of shortwave radiation on snow cover simulations to address this objective.

The importance of characterizing the effects of spatial scale has been an active area of hydrological research (Gupta et al. 1986; Wood et al. 1990; Sivapalan and Kalma 1995; Seyfried and Wilcox 1995; Bloschl and Sivapalan 1995; Wood et al. 1988). The scale impacts for snow hydrology, in particular, have also been examined in a number of studies (e.g., Bloschl 1999; Erickson et al. 2005; Trujillo et al. 2009) using techniques ranging from statistical modeling to analysis methods in the spectral domain. In this article, we use a scale decomposition approach using two-dimensional discrete Haar wavelet analysis to quantify how the improvements in snow cover simulations through topographic adjustments of solar input translate to different spatial scales.

Two midlatitude regional domains with complex topography at 1-km spatial resolution over Afghanistan and Colorado in the United States are chosen as the study areas. Two versions of the Noah LSM are used to simulate the fractional snow cover estimates. The simulations are conducted with and without topographic adjustments to the input radiation, over three snow seasons. The simulated snow cover fields are evaluated against the high-resolution snow covered area product from the Moderate Resolution Imaging Spectroradiometer (MODIS) optical sensor on the *Terra* spacecraft. In addition to evaluating the impact of spatial scales on

snow cover improvements, a separate analysis is conducted to assess the relative importance of precipitation inputs and the topographic correction to radiation on snow cover simulations.

This paper is organized as follows. We first describe the methodology for applying terrain adjustments to the downwelling shortwave radiation in section 2. This is followed by the description of experiments conducted over two study areas in section 3. Section 4 describes the evaluation methods and the results, and conclusions are presented in section 5.

2. Approach

To correct the downward incident surface solar radiation on a flat surface under given atmospheric conditions for terrain slope and orientation (aspect), it is first separated into direct and diffuse components. The direct component is able to penetrate through the atmosphere without getting attenuated by the particulates and clouds. The diffuse radiation, on the other hand, gets scattered by gases in the atmosphere. The parameterizations developed by Goudriaan (1977) and used by Sellers et al. (1986) for the Simple Biosphere Model (SiB) are used to partition the incident shortwave radiation (SW↓) into direct (SW_{direct}) and diffuse ($SW_{diffuse}$) components. The slope-aspect correction is then applied to correct the SW_{direct} component. The diffuse component is assumed to have no directional dependence by the time it reaches the earth's surface and no topographical adjustments are made to it.

The direct component is corrected for terrain based on slope and aspect (Dingman 2002; Frankenstein and Koenig 2004). The corrected direct shortwave flux is computed as

$$SW'_{direct} = SW_{direct}\left[\cos(\beta) + \frac{\sin(\theta)\sin(\beta)\cos(\alpha_r)}{\cos(\theta)}\right], \quad (1)$$

where β is the slope of the surface, θ is the solar zenith angle, and α_r is the relative aspect defined as the difference ($\alpha - \alpha_o$) between the aspect of the surface α relative to the north and solar aspect α_o relative to the north. The solar aspect α_o is calculated as

$$\alpha_o = \cos^{-1}\frac{[\sin(\Lambda)\cos(\theta) - \sin(\delta)]}{\cos(\Lambda)\sin(\theta)}, \quad (2)$$

where Λ is the latitude and δ is the declination of the sun. The corrected downward shortwave flux for a sloping surface is then computed as

$$SW'\downarrow = SW'_{direct} + SW_{diffuse}. \quad (3)$$

As explained in the following sections, land surface model simulations are conducted with and without the correction to the downward shortwave flux, and the corresponding impacts on the snow cover simulations are examined.

3. Experiment setup

The influence of terrain aspect for radiation adjustment is most important in the midlatitudes. At the equatorial regions, all slopes receive the same amount of radiation, as the sun is nearly overhead throughout different seasons. Over the arctic latitudes, the sun is too low on the horizon during the winter to provide enough radiation, whereas during the summer and spring, all slopes receive radiation of similar intensity when summed through the long solar days. During the winter season in the Northern Hemisphere, the amount of incident radiation on the north-facing slopes is less compared to that on the south-facing slopes. These effects are reversed in the Southern Hemisphere, with south-facing slopes receiving less radiation than the north-facing slopes. Here we consider two midlatitude regional domains in the Northern Hemisphere (Fig. 1) at 1-km spatial resolution: 1) a domain of 1600 km × 1200 km for the Colorado headwater region (CHR) centered around Colorado and 2) a domain of 1200 km × 1000 km over Afghanistan (AFG). The terrain in both simulation domains is complex, with the elevation ranges from 1000 to 6000 m. In CHR, the western and central parts are dominated by the mountainous terrain of the Rocky Mountains, whereas the Hindu Kush and Pamir mountains dominate the northeast parts of the AFG domain.

The LSM simulations are conducted using the National Aeronautics and Space Administration (NASA) Land Information System (LIS; Kumar et al. 2006) with two versions of the Noah LSM (versions 2.7.1 and 3.1; Ek et al. 2003), forced with both the corrected and the uncorrected radiation inputs. Noah includes a single layer snow submodel, which simulates the physical processes of temporally varying snow density and SWE. The fractional snow cover is then diagnosed from SWE (Koren et al. 1999; Livneh et al. 2010). The newer version of the Noah LSM (version 3.1) includes several snow physics–related enhancements, such as improvements to snow albedo specification and modifications to roughness length in the presence of snow (Barlage et al. 2010). The use of the different versions of the model also enables the evaluation of the impacts of these recent changes to the Noah snow physics. Noah requires the following meteorological variables as boundary conditions: downward shortwave radiation, downward longwave radiation, near-surface air temperature, near-surface specific

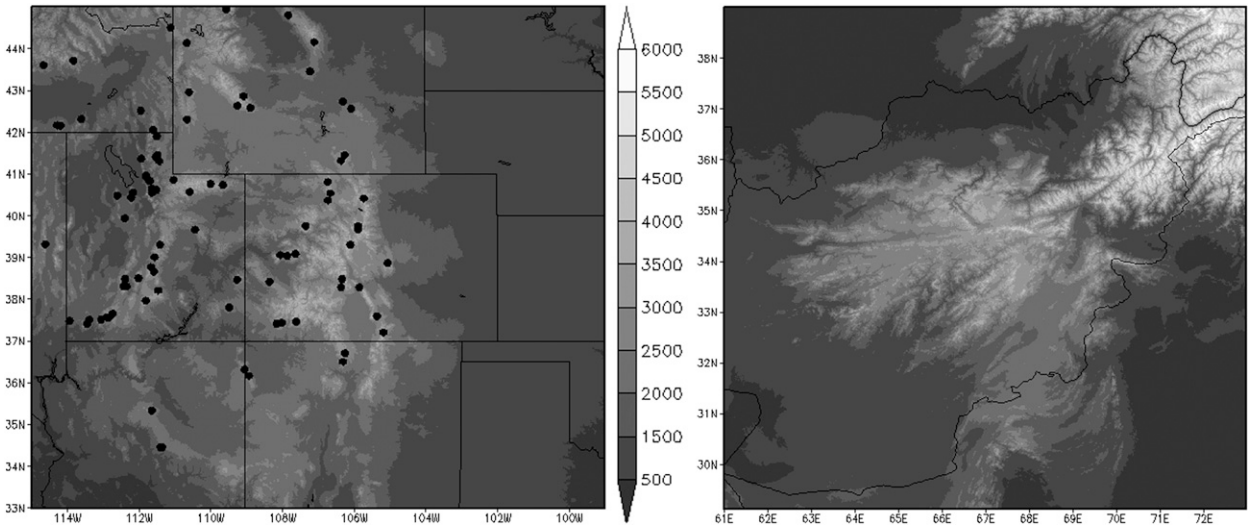

FIG. 1. The two study domains with 1-km terrain elevation as the background: (left) CHR domain and (right) AFG domain. The circles in the CHR domain represent the locations of the SNOTEL stations.

humidity, surface pressure, wind, and precipitation. The LSMs are driven with meteorological data from the Global Data Assimilation System (GDAS), the global meteorological weather model of NCEP (Derber et al. 1991). In addition, the precipitation inputs for the model simulations are provided from the National Oceanic and Atmospheric Administration (NOAA) Climate Prediction Center's (CPC) operational global 2.5° 5-day Merged Analysis of Precipitation (CMAP) (Xie and Arkin 1997), which is a product that employs blended satellite (IR and microwave) and gauge observations. The GDAS modeled precipitation fields are used to disaggregate the CMAP fields spatially and temporally to match the Noah model simulation resolutions. To investigate the impact of improved precipitation inputs on the simulations, the NLDAS Phase 2 (NLDAS-2; Xia et al. 2011) products are employed in a separate set of simulations. The LSM simulations use a time step of 30 min and are used to generate estimates of snow conditions (pixel SWE, pixel fSCA, and pixel snow depth) for three winter seasons, from 1 November 2007 to 1 May 2010. The model outputs are generated daily at the local MODIS overpass time [1030 local time (LT)] for each simulation domain.

The global, high-resolution (30-m resolution) elevation data from the Shuttle Radar Topography Mission (SRTM; Rodriguez et al. 2005) are used to derive the topography datasets of elevation, slope, and aspect at 1-km spatial resolution. These SRTM-based topography datasets are used to perform the spatial downscaling of downward shortwave fluxes, using the approach described in section 2.

Satellite-based and in situ measurements of snow conditions are used to evaluate the LSM simulations. The fractional snow cover extent global 500-m product [MODIS/*Terra* Snow Cover Daily L3 Global 500-m Grid (MOD10A1) version 5] (Hall et al. 2006), based on an algorithm of Salomonson and Appel (2004), from the MODIS instrument on the *Terra* spacecraft is used as the reference data for evaluating the snow cover simulations. The MOD10A1 product is aggregated (by simple averaging) to 1-km spatial resolution for enabling the comparisons presented in this article. In the CHR domain, in situ measurements of SWE are available from the Natural Resources Conservation Service (NRCS) Snowpack Telemetry (SNOTEL) meteorological stations. We employ these observations to evaluate the SWE fields from the model simulations.

4. Methods

a. Evaluation of snow cover simulations using categorical measures

Similar to the strategy followed in Dong and Peters-Lidard (2010), categorical verification measures are used to evaluate the snow cover simulations. Using a 2×2 contingency table approach (e.g., Painter et al. 2009) and a prescribed threshold, the snow cover model output and the MOD10A1 data are converted to a dichotomous ("yes" or "no") form. For example, if the threshold is defined as 0.1 for fractional snow cover, then all model fSCA outputs with values >0.1 are categorized as yes events and all values with <0.1 are categorized as no

TABLE 1. The 2 × 2 contingency table used to define the skill measures.

		Model output	
		fSCA > Threshold	fSCA ≤ Threshold
MOD10A1	fSCA > Threshold	TP	FN
	fSCA ≤ Threshold	FP	TN

events. Similarly, the corresponding observational data are categorized into yes and no events to complete the entries of the contingency table, shown in Table 1. Note that, effectively, a binary form of the MOD10A1 product that simply stipulates the presence or absence of snow is used in the comparisons presented in the article. TP represents true positives (when both the fSCA from the model and the observation are above the specified threshold), TN represents true negatives (when both fSCA from the model and observation are below the specified threshold), FN denotes false negatives (where fSCA from the model and observation are below and above the specified threshold, respectively), and FP represents false positives (where fSCA from the model and observation are above and below the specified threshold, respectively). The appendix describes a number of categorical skill measures based on the contingency table that are used in the analysis (Jolliffe and Stephenson 2012).

We focus primarily on two metrics: 1) the probability of detection of yes events (PODy), which measures the fraction of snow cover presence that was correctly simulated, and 2) false alarm ratio (FAR), which measures the fraction of no-snow events that was incorrectly simulated. As MODIS snow estimation over forested domains is known to have problems (Hall and Riggs 2007), we exclude the comparisons over grid points with forest cover. Grid points with cloud obscuration are masked out based on the MODIS cloud mask data product (MOD35_L2). In the comparisons, the model outputs are matched to the local overpass time of the satellite measurements, which is assumed to be at 1030 LT in each domain. Note that all categorical metrics are computed separately for each grid point in the domain, though the following sections primarily focus on the presentation of domain averages. The number of pixels used to calculate the metric values depends on the number of available MODIS snow cover pixels. For the AFG and CHR domains, roughly 15% and 40%, respectively, of the domain has cloud-free observations. To reduce the statistical artifacts of the number of sampled points in computing domain averages, we applied a minimum threshold of available grid points to be 10% and 20% of the total domain for AFG and CHR, respectively, for determining valid estimates of performance metrics.

To quantify the improvements due to the topographic correction, we define a ''Delta metric'' as the difference between the metric values of the model simulations with and without topographic correction. An improved model should increase POD and decrease the FAR. For the PODy, ''DeltaPODy'' is defined as the PODy of the integration with correction minus the PODy of the integration without correction. For FAR, ''DeltaFAR'' is defined as the FAR of the simulation without correction minus the FAR of the simulation with correction. As a result, if the topographic correction improves the metric (increases PODy and reduces FAR), then DeltaPODy and DeltaFAR will be positive. On the other hand, Delta metrics will be negative if the topographic correction degrades the snow cover estimates.

b. *Scale decomposition analysis of improvements in snow cover simulation*

The intensity-scale approach of Casati et al. (2004), originally developed for the spatial verification of precipitation forecasts, is used to perform the scale decomposition of the snow cover improvement fields for PODy and FAR. Using a predefined threshold, the PODy and FAR fields from the corrected (C) and uncorrected (UC) simulations are converted into binary fields, I_C and I_{UC}, respectively. In the comparisons presented here, a threshold value of 0.1 was used. The difference between these intensity fields is then defined as the binary error field ($Z = I_C - I_{\mathrm{UC}}$).

A two-dimensional Haar wavelet decomposition is performed to decompose the binary error field into the sum of components at different spatial scales, which are orthogonal (Mallat 1989). As the algorithm computes successive decompositions by the powers of 2, the size of the initial binary field must also be a power of 2. The binary field Z (defined at 1 km in this instance) is first converted into a field of $2^L \times 2^L$ grid points by padding the domain with fill data to the nearest dimension of 2^L. In these comparisons, zeroes are used to pad the domain. Applying the Haar wavelet filter decomposes this binary field into ''father'' and ''mother'' wavelet components, representing the coarser mean field and the variation-about-the-mean fields, respectively (at 2-km spatial resolution). The father wavelet component is further decomposed into a coarser (4-km resolution) field by applying the Haar wavelet transform. This process is repeated L times, generating father and mother wavelet components at each step. The binary field Z can be expressed as the sum of the mother wavelet components at the spatial scales $l = 1, \ldots, L$.

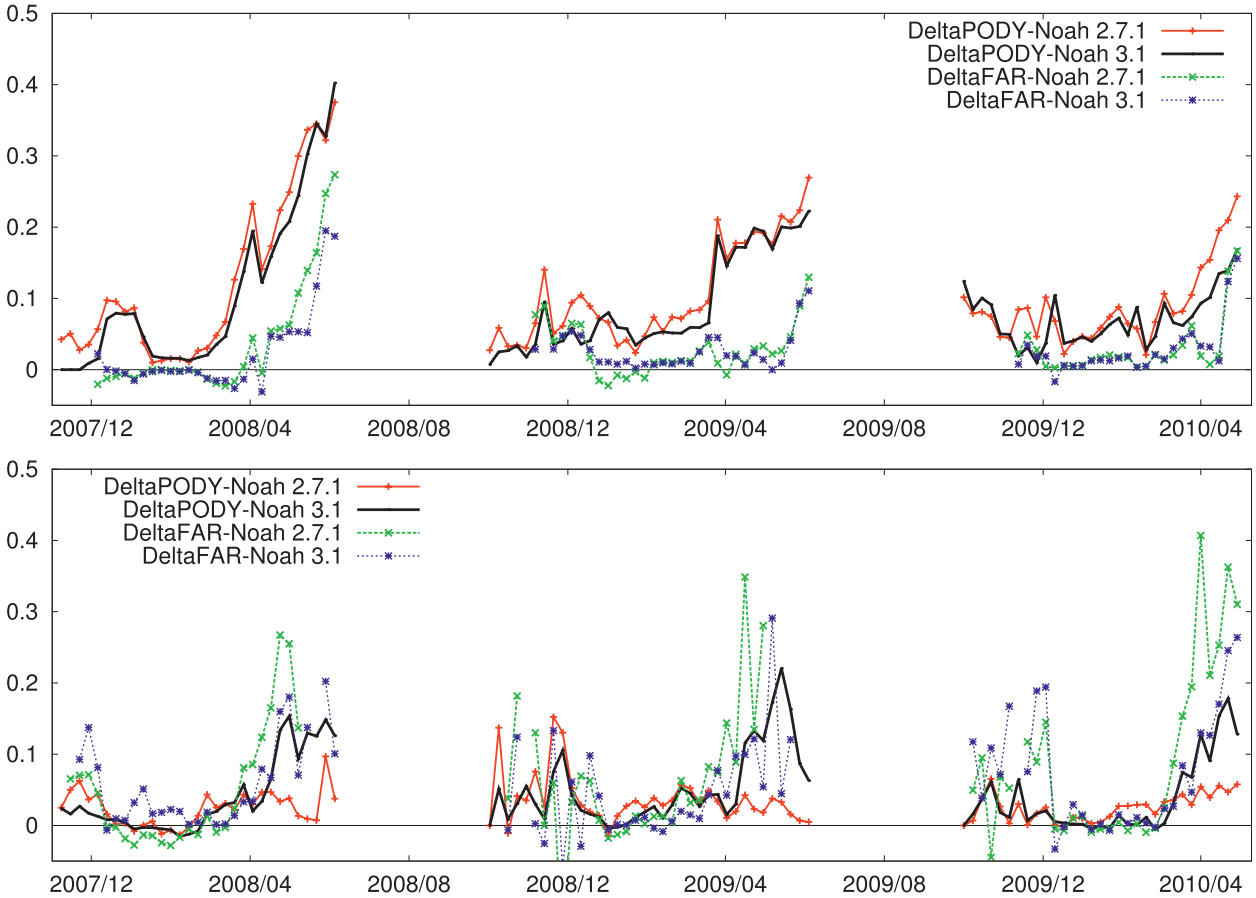

FIG. 2. Time series of the DeltaPODy [PODy(C) − PODy(UC)] and DeltaFAR [FAR (UC) − FAR(C)] of snow cover from the LSM simulations compared against MOD10A1: (top) AFG domain and (bottom) CHR domain.

In the intensity-scale verification method proposed by Casati et al. (2004), the mean squared error (MSE) of the binary field is computed at each spatial scale, as the average of the squared differences over all the grid points in the domain. The MSE of the binary field is equal to

$$\mathrm{MSE} = \sum_{l=1}^{L} \mathrm{MSE}_l, \tag{4}$$

where $\mathrm{MSE}_l = \overline{Z_l^2}$ is the MSE of the lth spatial scale component of the binary field.

5. Results

a. *Evaluation of snow cover simulations using categorical measures*

Figure 2 shows the time series of domain-averaged DeltaPODy and DeltaFAR for both AFG and CHR domains. The Delta values are computed using the weekly average of daily PODy and FAR values. In this comparison, a detection threshold of 0.8 is used to compute the PODy and FAR values. For example, a correct simulation of fSCA is assumed when both model and observations indicate fSCA values above 0.8. Sensitivity of the results to other threshold values was also examined and is described below. Figure 2 indicates that the Delta metric is generally positive throughout the 3-yr simulation time period, suggesting that the topographic correction to shortwave radiation translates to systematic improvements in the snow cover simulations. The observed improvement trends are similar in both versions of Noah, which suggest that the improvements to snow cover simulation through topographic adjustments are retained as added enhancements on top of the newer physics. The terrain-based correction of radiation provides the most improvements in snow cover simulations during the snow accumulation and melt periods. The improvements in PODy and FAR for the three snow seasons are compared here to demonstrate that the topographic adjustments to radiation lead to systematic

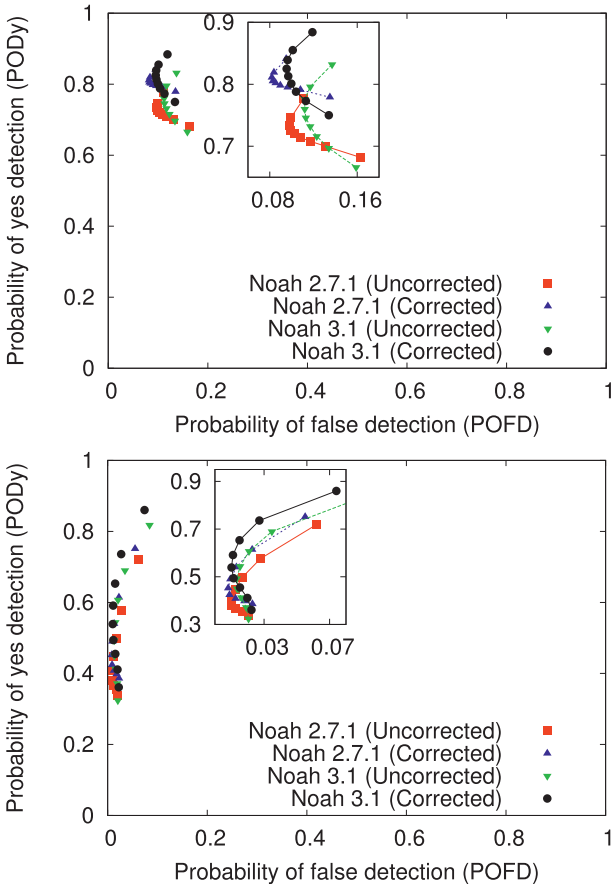

FIG. 3. Comparison of the influence of different detection thresholds in evaluating modeled snow cover estimates. The plotted points in the ROC space characterize the tradeoffs between POFD and PODy when different detection thresholds are used to compute the metrics: (top) AFG domain and (bottom) CHR domains.

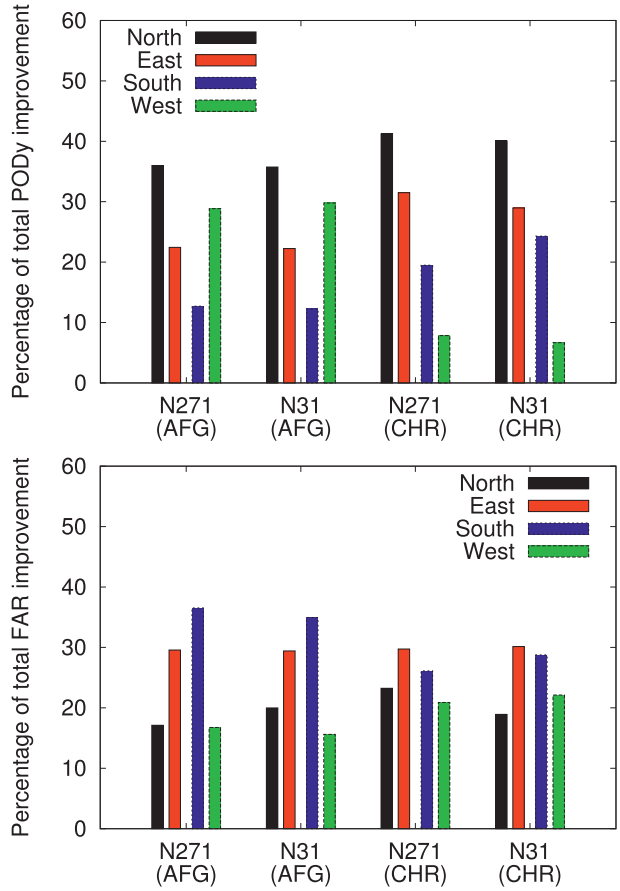

FIG. 4. The improvements in (top) PODy and (bottom) FAR stratified by the four cardinal aspect directions for both study regions and two land surface models, Noah version 2.7.1 (N271) and Noah version 3.1 (N31).

improvements in snow cover fields, irrespective of the interannual variations in the snow cover estimates.

Figure 3 shows the performance of the model simulations in the receiver operating characteristic (ROC) space when different threshold values are used to compute the contingency-table-based metrics. ROC space is used to compare the true positive rate (PODy) against false positive rate (POFD). The threshold values used to compute the metrics are varied from 0.1 to 0.9, and the resulting pairs of PODy and POFD values are plotted in the ROC space. The predictions close to the upper-left corner (0, 1) of the ROC space represent a small number of false negatives and a high number of true positives. The diagonal and lower triangular regions of the ROC space represent areas with no skill and worse skill, respectively. As seen in Fig. 3, all model simulations are in the upper-left corner, indicating high skills in snow cover simulations. The topographic correction further pushes these pairs closer to the (0, 1) corner, representing the added improvement from topographic correction on snow cover simulations. These trends are observed in both AFG and CHR domains, for both LSMs, with the contrast between the corrected and uncorrected set of points more distinct in the AFG domain results. More importantly, the ROC space in Fig. 3 also demonstrates that skill improvements are obtained regardless of the chosen threshold value, though we use the value of 0.8 for describing most of the results in this manuscript.

The improvements in PODy and FAR stratified to the four cardinal aspect categories in each domain are shown in Fig. 4. The figure indicates that improvements in both PODy and FAR are obtained in all four aspect categories. As might be expected, the improvements in PODy are more prominent over the north-facing slopes in both domains, whereas the improvements in FAR are more prominent over the south-facing slopes. The effect of the terrain-based adjustments is to reduce the amount

TABLE 2. Domain-averaged skill metrics (all with 95% confidence intervals) for both AFG and CHR domains. The percent change is computed by subtracting the corrected column from the uncorrected column.

	Afghanistan					
	Noah 2.7.1			Noah 3.1		
	Uncorrected	Corrected	Change (%)	Uncorrected	Corrected	Change (%)
PODy	$0.700 \pm 1 \times 10^{-3}$	$0.791 \pm 1 \times 10^{-3}$	13.0	$0.697 \pm 1 \times 10^{-3}$	$0.773 \pm 1 \times 10^{-3}$	10.9
FAR	$0.202 \pm 1 \times 10^{-3}$	$0.189 \pm 1 \times 10^{-3}$	−6.4	$0.209 \pm 1 \times 10^{-3}$	$0.198 \pm 1 \times 10^{-3}$	−5.2
POFD	$0.131 \pm 5 \times 10^{-4}$	$0.108 \pm 5 \times 10^{-4}$	−17.5	$0.134 \pm 5 \times 10^{-4}$	$0.113 \pm 5 \times 10^{-4}$	−15.7
ACC	$0.793 \pm 5 \times 10^{-4}$	$0.821 \pm 5 \times 10^{-4}$	3.5	$0.790 \pm 5 \times 10^{-4}$	$0.813 \pm 5 \times 10^{-4}$	2.9
CSI	$0.581 \pm 8 \times 10^{-4}$	$0.630 \pm 8 \times 10^{-4}$	8.4	$0.572 \pm 7 \times 10^{-4}$	$0.615 \pm 7 \times 10^{-4}$	7.5
ETS	$0.371 \pm 1 \times 10^{-3}$	$0.429 \pm 1 \times 10^{-3}$	15.6	$0.365 \pm 1 \times 10^{-3}$	$0.411 \pm 1 \times 10^{-3}$	12.6
	Colorado headwater region					
	Noah 2.7.1			Noah 3.1		
	Uncorrected	Corrected	Change (%)	Uncorrected	Corrected	Change (%)
PODy	$0.354 \pm 1 \times 10^{-3}$	$0.398 \pm 1 \times 10^{-3}$	12.4	$0.372 \pm 1 \times 10^{-3}$	$0.411 \pm 1 \times 10^{-3}$	10.5
FAR	$0.233 \pm 1 \times 10^{-3}$	$0.224 \pm 1 \times 10^{-3}$	−3.9	$0.298 \pm 1 \times 10^{-3}$	$0.284 \pm 1 \times 10^{-3}$	−4.7
POFD	$0.017 \pm 1 \times 10^{-4}$	$0.018 \pm 1 \times 10^{-4}$	5.9	$0.019 \pm 1 \times 10^{-4}$	$0.020 \pm 1 \times 10^{-4}$	5.3
ACC	$0.880 \pm 1 \times 10^{-4}$	$0.883 \pm 1 \times 10^{-4}$	0.3	$0.878 \pm 1 \times 10^{-4}$	$0.880 \pm 1 \times 10^{-4}$	0.2
CSI	$0.143 \pm 3 \times 10^{-4}$	$0.144 \pm 3 \times 10^{-4}$	0.7	$0.109 \pm 3 \times 10^{-4}$	$0.110 \pm 3 \times 10^{-4}$	0.9
ETS	$0.035 \pm 1 \times 10^{-4}$	$0.036 \pm 1 \times 10^{-4}$	2.9	$0.034 \pm 1 \times 10^{-4}$	$0.037 \pm 1 \times 10^{-4}$	8.8

of incident radiation on the north-facing slopes. As a result, the amount of snowmelt (over the north-facing slopes) in the corrected simulations will be less, leading to higher PODy values. Conversely, the terrain-based correction increases the amount of incident radiation on the south-facing slopes, leading to more snowmelt. This, in turn, leads to reducing the FAR estimates. These characteristics are seen in the improvement trends in Fig. 4, which show higher contribution to DeltaPODy values from the north-facing slopes and higher contribution to DeltaFAR values from the south-facing slopes. In the AFG domain, the percentage of west-facing slopes is higher, whereas the percentage of east-facing slopes is higher in the CHR domain. The larger number of grid points in these aspect categories contributes to the corresponding increased contribution to PODy and FAR improvement values for these categories (Fig. 4).

Table 2 presents the domain-averaged statistics of various categorical measures from the suite of simulations (using a detection threshold of 0.8) for both modeling domains across the 3-yr analysis period. The table also lists the associated 95% confidence intervals associated with each metric. Note that any spatial autocorrelation of the skill values across the domain is ignored in computing these confidence intervals. The intervals reported here are likely to be larger if allowance for spatial autocorrelation of errors is included in the confidence interval computations. Except in the case of the POFD metric for the CHR domain (where there is a marginal degradation), topographic correction provides improvements across all evaluation metrics, for both LSMs. The improvements in snow cover detection are confirmed by the increase in PODy and reduction in FAR and POFD. The improvement in accuracy is demonstrated by the increase in values of accuracy measure (ACC), critical success index (CSI) and equitable threat score (ETS) metrics. Generally, Noah 2.7.1's performance is better than that of Noah 3.1 over AFG, but over CHR Noah 3.1 simulations are improved over Noah 2.7.1, consistent with the findings of Barlage et al. (2010) and Livneh et al. (2010). Nevertheless, the topographic correction of radiation provides improvements in both LSM versions. Further, all improvement trends are observed to be statistically significant. Note that these summary statistics are computed across the whole domain and across the whole 3-yr simulation period. As most of the improvements due to topographic correction occur during the accumulation and melt periods (Fig. 2), the summary statistics in Table 2 are recomputed by excluding the peak winter months of December, January, and February and are shown in Table 3. The improvements in snow cover simulations are more magnified if the analysis is restricted to transient snow periods. For example, over Afghanistan there is an overall 13% improvement in PODy and 6.4% improvement in FAR for Noah 2.7.1. For the same LSM and domain, these improvements increase to 40.2% in PODy and 14% in FAR, if only the transient snow periods are considered. Similar trends can be observed in other metrics in Tables 2 and 3, providing further confirmation that the topographic adjustments to radiation are more beneficial during the accumulation and melt periods.

TABLE 3. As in Table 2, but stratified for the transient snow periods.

	Afghanistan					
	Noah 2.7.1			Noah 3.1		
	Uncorrected	Corrected	Change (%)	Uncorrected	Corrected	Change (%)
PODy	$0.485 \pm 2 \times 10^{-3}$	$0.680 \pm 2 \times 10^{-3}$	40.2	$0.541 \pm 2 \times 10^{-3}$	$0.691 \pm 1 \times 10^{-3}$	27.7
FAR	$0.243 \pm 2 \times 10^{-3}$	$0.209 \pm 2 \times 10^{-3}$	−14.0	$0.231 \pm 1 \times 10^{-3}$	$0.199 \pm 1 \times 10^{-3}$	−13.8
POFD	$0.092 \pm 5 \times 10^{-4}$	$0.075 \pm 5 \times 10^{-4}$	−18.5	$0.101 \pm 5 \times 10^{-4}$	$0.085 \pm 5 \times 10^{-4}$	−15.8
ACC	$0.800 \pm 7 \times 10^{-4}$	$0.830 \pm 7 \times 10^{-4}$	3.8	$0.809 \pm 5 \times 10^{-4}$	$0.830 \pm 5 \times 10^{-4}$	2.6
CSI	$0.292 \pm 1 \times 10^{-3}$	$0.359 \pm 1 \times 10^{-3}$	22.9	$0.326 \pm 1 \times 10^{-3}$	$0.379 \pm 1 \times 10^{-3}$	16.3
ETS	$0.126 \pm 1 \times 10^{-3}$	$0.181 \pm 1 \times 10^{-3}$	43.7	$0.145 \pm 1 \times 10^{-3}$	$0.189 \pm 1 \times 10^{-3}$	30.3
	Colorado headwater region					
	Noah 2.7.1			Noah 3.1		
	Uncorrected	Corrected	Change (%)	Uncorrected	Corrected	Change (%)
PODy	$0.181 \pm 1 \times 10^{-3}$	$0.285 \pm 2 \times 10^{-3}$	57.5	$0.246 \pm 1 \times 10^{-3}$	$0.389 \pm 2 \times 10^{-3}$	58.1
FAR	$0.173 \pm 1 \times 10^{-3}$	$0.153 \pm 1 \times 10^{-3}$	−11.6	$0.176 \pm 3 \times 10^{-3}$	$0.162 \pm 2 \times 10^{-3}$	−8.0
POFD	$0.003 \pm 1 \times 10^{-4}$	$0.003 \pm 1 \times 10^{-4}$	0.0	$0.006 \pm 4 \times 10^{-5}$	$0.006 \pm 4 \times 10^{-5}$	0.0
ACC	$0.943 \pm 1 \times 10^{-4}$	$0.946 \pm 1 \times 10^{-4}$	0.30	$0.946 \pm 1 \times 10^{-4}$	$0.950 \pm 1 \times 10^{-4}$	0.40
CSI	$0.049 \pm 2 \times 10^{-4}$	$0.052 \pm 2 \times 10^{-4}$	6.1	$0.071 \pm 3 \times 10^{-4}$	$0.078 \pm 3 \times 10^{-4}$	9.9
ETS	$0.005 \pm 1 \times 10^{-4}$	$0.007 \pm 1 \times 10^{-4}$	40.0	$0.017 \pm 1 \times 10^{-4}$	$0.021 \pm 1 \times 10^{-4}$	23.5

In addition to the evaluation of snow cover estimates, in situ measurements of snow conditions are used to evaluate the modeled SWE estimates. The summary of the evaluation of the SWE fields from the model simulations against in situ measurements is presented in Table 4. The SNOTEL stations in the CHR domain are chosen such that they are located over pixels with large slopes (and not over flat terrain), where the topographic correction would affect the incident solar radiation. The locations of the stations are shown in Fig. 1. Table 4 presents the domain-averaged RMSE and bias errors from different model simulations compared against these in situ measurements, along with the associated 95% confidence intervals. The errors in the SWE estimates are large, possibly because of the representativeness errors introduced by the coarse forcing inputs and the spatial resolution of the modeling domain. Nevertheless, statistically significant and systematic reduction in RMSE and bias errors are observed in the modeled SWE fields as a result of the terrain-based correction of radiation. These trends confirm that the terrain-based correction of radiation helps in not only improving snow cover simulations, but also in improving the SWE estimates. The snow depth measurements from NOAA's Cooperative Observer Program (COOP) (Quayle et al. 1991) stations were also used to evaluate the modeled snow depth fields. The trends in snow depth fields were found to be statistically insignificant, as a result of the lack of adequate sampling density in the measurements from the available COOP stations. As a result, these comparisons are not shown. Table 4 also indicates that there is only a marginal improvement in the Noah 3.1 SWE simulation compared to the Noah 2.7.1 estimates, and these trends are not statistically significant. In this instance, the improvements in SWE simulations from topographic adjustments to solar inputs are more significant than the improvements due to model physics changes.

b. *Scale decomposition analysis of improvements in snow cover simulation*

To analyze how the improvements in snow cover estimates obtained at 1 km translate to other spatial resolutions, we apply the scale decomposition analysis. For simplicity, we limit the analysis to the DeltaPODy and DeltaFAR metrics only. Using the approach mentioned in section 4, the two-dimensional Haar wavelet decomposition is used to decompose the 1-km fields of DeltaPODy and DeltaFAR to sum the components at different spatial scales (at 2, 4, 8, 16, up to 1024 km). The mean squared error of the binary fields at each spatial scale is computed and the percentage contribution of each spatial scale to the total improvement is computed as $(\mathrm{MSE}_l \times 100)/\mathrm{MSE}$, for $l = 1, \ldots, L$, with L being 9 ($2^9 = 1024$).

TABLE 4. Domain-averaged error metrics (all with 95% confidence intervals) for the CHR domain compared against in situ SNOTEL SWE measurements.

	Noah 2.7.1		Noah 3.1	
	Uncorrected	Corrected	Uncorrected	Corrected
RMSE (mm)	276 ±18	248 ±18	269 ±18	246 ±20
Bias (mm)	−188 ±13	−163 ±13	−183 ±13	−160 ±15

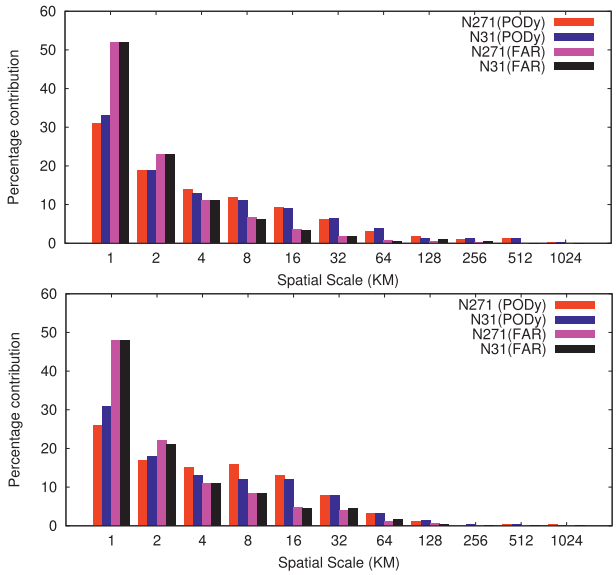

FIG. 5. Percentage contribution to the total improvements in PODy and FAR at different spatial scales generated by a two-dimensional discrete Haar wavelet analysis: (top) AFG domain and (bottom) CHR domain.

Figure 5 shows the result of scale decomposition of the total improvement fields for PODy and FAR for both domains using the two land surface models. The bars in the figure present the percentage contribution of each scale to the total improvement. The trends in scale decomposition of DeltaPODy and DeltaFAR fields are similar across both LSMs and the two domains. As expected, most of the improvements in PODy and FAR are provided by the fine scales, and it decreases rapidly at coarser scales. Approximately 30% of the improvements in PODy and 50% of the improvements in FAR are a function of the 1-km scale alone. At resolutions coarser than 16 km, the percentage contribution of the scale drops to below 10% for PODy. For FAR, the contribution of the spatial scale is largely limited to resolutions 4 km and finer. This result provides an indicator of the spatial scale at which improvements can be expected as a result of topographic correction to radiation. For example, land surface modeling domains such as NLDAS, which use a spatial resolution of 12.5 km, should include the topographic adjustments to radiation, as the expected PODy improvements in snow cover simulation are above 10%.

c. *Evaluation of the relative influence of precipitation*

As seen in Fig. 2, the trends in the improvements of PODy and FAR indicate significant interannual variability. These variations can be caused by several factors, including the interannual variability in the forcing meteorology. Since precipitation is a key input that affects the evolution of snow fields, here we investigate its relative influence on the improvement trends of categorical metrics using the factor separation analysis of Stein and Alpert (1993).

TABLE 5. Structure of experiments for the factor separation analysis and the definition of contribution factors.

Factor	Precipitation forcing	Topographic correction
$F0$	CMAP	No
$F1$	CMAP	Yes
$F2$	NLDAS	No
$F12$	NLDAS	Yes
Difference	Represents	
$f1 = F1 - F0$	Contribution of topographic correction	
$f2 = F2 - F0$	Contribution of precipitation	
$f12 = F12 - (F1 + F2) + F0$	Contribution of the joint influence of topographic correction and precipitation	

To assess the sensitivity of snow cover estimates to precipitation, a set of additional model simulations is conducted over the CHR domain by changing the precipitation input to the NLDAS-2 (Xia et al. 2011) data but keeping all other meteorological inputs same as those described in section 3. As above, model simulations are conducted using both versions of the Noah LSM, with and without the topographic correction of radiation. These sets of experiments allow the investigation of the sensitivity of three factors contributing to the snow evolution: 1) influence of precipitation, 2) influence of topographic correction to radiation, and 3) the joint influence of precipitation and topographic correction to radiation. Table 5 presents the setup of experiments conducted with each LSM. The categorical metric values (e.g., PODy and FAR) are computed for each experiment, and the corresponding contribution factors ($f1$, $f2$, and $f12$) are computed.

Figure 6 presents the results of the factor separation analysis for both versions of the Noah LSM. The results indicate that the influence of precipitation (factor $f1$) is most significant across all of the evaluation metrics and that the contribution due to topographic correction of radiation (factor $f2$) is smaller compared to the precipitation influence. Finally, the influence of the joint influence term (factor $f12$) is also small in all evaluation metrics. The NLDAS precipitation is generally considered to be a higher-quality product compared to CMAP (Matsui et al. 2010). The NLDAS-2 precipitation over the continental United States uses monthly Parameter-Elevation Regressions on Independent Slopes Model (PRISM) (Daly et al. 1994) adjustments for orographic precipitation impacts. This analysis suggests that the

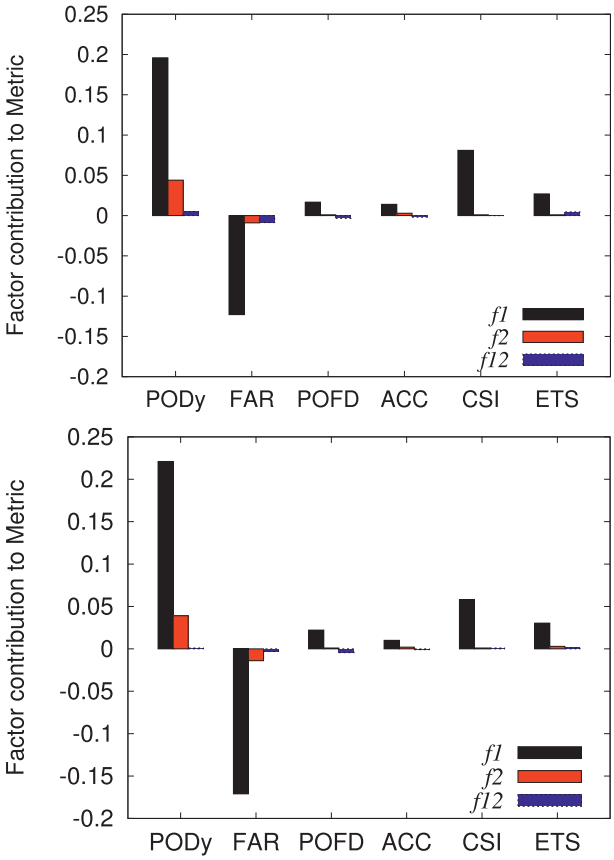

FIG. 6. Relative influence of precipitation input ($f1$), topographic correction of radiation ($f2$), and the joint influence of precipitation and topographic correction of radiation ($f12$) in snow cover evaluation metrics using the factor separation analysis. Analysis shown for Noah versions (top) 2.7.1 and (bottom) 3.1.

improvements in snow cover simulations obtained with the use of a more accurate precipitation input has a greater impact than the topographic correction of radiation on snow cover simulations. Nevertheless, in areas such as Afghanistan where high-quality precipitation inputs are not typically available, the terrain-based adjustments to radiation can be a viable approach for generating improvements in snow cover estimates.

6. Summary

This article presents a multiscale evaluation of the impact of terrain-based correction of shortwave radiation on snow simulations. The evaluation is performed over two midlatitude domains at 1-km spatial resolution near Afghanistan and the Colorado headwater region using two versions of the Noah land surface model. The snow cover simulations are evaluated by comparing them against the snow cover observations from MODIS. The evaluations indicate systematic improvements in snow cover estimates in both LSMs, with increased PODy and reduced FAR in the simulations that employ terrain-corrected shortwave radiation inputs. The improvements to PODy and FAR are more significant during the snow accumulation and melt periods; the improvements are consistently observed when different detection thresholds are used to compute the evaluation metrics.

The terrain-based correction to the shortwave radiation adjusts the downwelling radiation by reducing the incident amount over north-facing slopes, increasing the incident amount over south-facing slopes, and causing diurnal adjustments over east- and west-facing slopes. Improvements in snow cover estimates were observed in all four cardinal slope directions as a result of the radiation adjustments. More improvements for PODy and FAR are observed over the north- and south-facing slopes, respectively. Similar trends confirming the positive impact of terrain-based correction of shortwave radiation are observed when accuracy measures such as critical success index and equitable threat scores are used to evaluate the simulations. Finally, the comparison of the modeled SWE fields against in situ SNOTEL observations further confirms that the terrain-based adjustments to radiation also translate to systematic, statistically significant improvements to the simulated SWE fields.

To understand how the improvements in snow cover simulations from terrain-based correction of radiation translate at other spatial scales, a two-dimensional discrete Haar wavelet analysis is conducted. The analysis separates the improvement field at 1 km into orthogonal subcomponents at coarser scales. For both domains, the contribution of the scale to PODy improvement falls below 10% at resolutions coarser than 16 km. For FAR, at resolutions coarser than 4 km, the contribution to the total improvement is less than 10%. Therefore, one can conclude from this analysis that land surface modeling domains with a horizontal spatial resolution of 16 km or finer over midlatitudes (e.g., NLDAS) should include topographic adjustments to radiation. To assess the relative influence of precipitation in the interannual variations, sensitivity experiments are conducted by using precipitation data from the NLDAS-2 project to force the LSMs over the CHR domain. A factor separation analysis conducted to quantify the relative influence of topographic correction and precipitation indicates the stronger influence of precipitation inputs in the snow estimates.

Acknowledgments. We gratefully acknowledge the financial support from the Air Force Weather Agency. Computing was supported by the resources at the NASA

Center for Climate Simulation. The NLDAS-2 data used in this effort were acquired as part of the activities of NASA's Science Mission Directorate and are archived and distributed by the Goddard Earth Sciences (GES) Data and Information Services Center (DISC).

APPENDIX

Definition of Categorical Skill Measures

Probability of detection of yes events (PODy) is

$$\mathrm{PODy} = \frac{\mathrm{TP}}{\mathrm{TP} + \mathrm{FN}}. \tag{A1}$$

PODy measures the fraction of observed events that were correctly predicted by the model. PODy ranges from 0 to 1 with a perfect simulation having a value of 1.

False alarm ratio (FAR) is

$$\mathrm{FAR} = \frac{\mathrm{FP}}{\mathrm{TP} + \mathrm{FP}}. \tag{A2}$$

FAR measures the fraction of model predictions that were observed to be nonevents. The range of FAR is from 0 to 1, with 0 being the desired value.

Probability of false detection (POFD) is

$$\mathrm{POFD} = \frac{\mathrm{FP}}{\mathrm{TN} + \mathrm{FP}}. \tag{A3}$$

POFD measures the fraction of false alarms given the event did not occur. Similar to FAR, the range of POFD is from 0 to 1, with a perfect simulation having a value of 0.

Accuracy measure (ACC) is

$$\mathrm{ACC} = \frac{\mathrm{TP} + \mathrm{TN}}{\mathrm{TP} + \mathrm{FP} + \mathrm{FN} + \mathrm{TN}}. \tag{A4}$$

ACC measures the fraction of events that were either true positives or true negatives. Its value ranges from 0 to 1, with a perfect simulation having an ACC value of 1.

Critical success index (CSI) is

$$\mathrm{CSI} = \frac{\mathrm{TP}}{\mathrm{TP} + \mathrm{FP} + \mathrm{FN}}. \tag{A5}$$

CSI defines the ratio of the number of times the observed event was correctly simulated to the number of times it was either simulated or observed. A CSI value of 1 indicates perfect model output. CSI accounts for both false alarms and missed events.

Equitable threat score (ETS) is

$$\mathrm{ETS} = \frac{\mathrm{TP} - C}{\mathrm{TP} + \mathrm{FP} + \mathrm{FN} - C}, \tag{A6}$$

where

$$C = \frac{(\mathrm{TP} + \mathrm{FP})(\mathrm{TP} + \mathrm{FN})}{\mathrm{TP} + \mathrm{FP} + \mathrm{FN} + \mathrm{TN}}. \tag{A7}$$

ETS is a modified form of the CSI metric, corrected for the true positives that would be expected by chance. A perfect simulation will have an ETS value of 1.

REFERENCES

Ackerman, S., K. Strabala, P. Menzel, R. Frey, C. Moeller, and L. Gumley, 1998: Discriminating clear sky from clouds with MODIS. *J. Geophys. Res.,* **103** (D24), 32 141–32 157.

Barlage, M., and Coauthors, 2010: Noah land surface model modifications to improve snowpack prediction in the Colorado Rocky Mountains. *J. Geophys. Res.,* **115,** D22101, doi:10.1029/2009JD013470.

Barnett, T., J. Adam, and D. Lettenmaier, 2005: Potential impacts of a warming climate on water availability in snow-dominated regions. *Nature,* **438,** 303–309, doi:10.1038/nature04141.

Bloschl, G., 1999: Scaling issues in snow hydrology. *Hydrol. Processes,* **13,** 2149–2175.

——, and M. Sivapalan, 1995: Scale issues in hydrological modeling: A review. *Hydrol. Processes,* **9,** 251–290.

Casati, B., G. Ross, and D. Stephenson, 2004: A new intensity-scale approach for the verification of spatial precipitation forecasts. *Meteor. Appl.,* **11,** 141–154, doi:10.1017/S1350482704001239.

Cline, D., 1997: Sub-resolution energy exchanges and snowmelt in a distributed SWE and snowmelt model for mountain basins. *Eos, Trans. Amer. Geophys. Union,* **78** (Fall Meeting Suppl.), Abstract H12B-10.

Cohen, J., and D. Entekhabi, 1999: Eurasian snow cover variability and Northern Hemisphere climate predictability. *Geophys. Res. Lett.,* **26,** 345–348.

Daly, C., R. Neilson, and D. Phillips, 1994: A statistical-topographic model for mapping climatological precipitation over mountainous terrain. *J. Appl. Meteor.,* **33,** 140–158.

Derber, J., D. Parrish, and S. Lord, 1991: The new global operational analysis system at the National Meteorological Center. *Wea. Forecasting,* **6,** 538–547.

Dingman, S., 2002: *Physical Hydrology*. 2nd ed. Prentice Hall, 646 pp.

Dong, J., and C. Peters-Lidard, 2010: On the relationship between temperature and MODIS snow cover retrieval errors in the western U.S. *IEEE Trans. Geosci. Remote Sens.,* **3,** 132–140.

Dozier, J., 1979: A solar radiation model for a snow surface in mountainous terrain. *Modeling Snow Cover Runoff,* S. Colbeck and M. Ray, Eds., U.S. Army Cold Regions Research and Engineering Laboratory, 144–153.

Ek, M., K. Mitchell, L. Yin, P. Rogers, P. Grunmann, V. Koren, G. Gayno, and J. Tarpley, 2003: Implementation of Noah land surface model advances in the National Centers for Environmental Prediction operational mesoscale Eta model. *J. Geophys. Res.,* **108,** 8851, doi:10.1029/2002JD003296.

Elder, K., W. Rosenthal, and R. Davis, 1998: Estimating the spatial distribution of snow water equivalence in a montane watershed. *Hydrol. Processes,* **12,** 1793–1808.

Erickson, T., M. Williams, and A. Winstral, 2005: Persistence of topographic controls on the spatial distribution of snow in rugged mountain terrain, Colorado, United States. *Water Resour. Res.,* **41,** W04014, doi:10.1029/2003WR002973.

Evans, B., D. Walker, D. Benson, E. Nordstrand, and G. Petersen, 1989: Spatial interrelationships between terrain, snow distribution and vegetation patterns at an arctic foothills site in Alaska. *Holarctic Ecol.,* **12,** 270–278.

Frankenstein, S., and G. Koenig, 2004: Fast all-season soil strength (FASST) model. Tech. Rep. SR-04-01, Cold Regions Research and Engineering Laboratory, U.S. Army Corps of Engineers, Hanover, NH, 86 pp.

Goudriaan, J., 1977: Crop micrometeorology: A simulation study. Tech. Rep., Center for Agricultural Publishing and Documentation, Wageningen, Netherlands, 249 pp.

Gupta, V., I. Rodriguez-Iturbe, and E. Wood, 1986: *Scale Problems in Hydrology*. D. Reidel, 246 pp.

Hall, D., and G. Riggs, 2007: Accuracy assessment of the MODIS snow products. *Hydrol. Processes,* **21,** 1534–1547.

——, ——, V. Salomonson, N. DiGirolamo, and K. Bayr, 2002: MODIS snow cover products. *Remote Sens. Environ.,* **83,** 181–194.

——, ——, and ——, 2006: MODIS/*Terra* snow cover daily L3 global 500m grid, version 5. National Snow and Ice Data Center, Boulder, CO, digital media. [Available online at http://nsidc.org/data/mod10a1v5.html.]

Helbig, N., and H. Löwe, 2012: Shortwave radiation parameterization scheme for subgrid topography. *J. Geophys. Res.,* **117,** D03112, doi:10.1029/2011JD016465.

Jolliffe, I., and D. Stephenson, Eds., 2012: *Forecast Verification: A Practitioner's Guide in Atmospheric Science*. 2nd ed. John Wiley & Sons, 274 pp.

Koren, V., J. Schaake, K. Mitchell, Q.-Y. Duan, F. Chen, and J. Baker, 1999: A parameterization of snowpack and frozen ground intended for NCEP weather and climate models. *J. Geophys. Res.,* **104,** 19 569–19 585.

Kumar, S., and Coauthors, 2006: Land information system: An interoperable framework for high resolution land surface modeling. *Environ. Model. Software,* **21,** 1402–1415.

Liston, G., and K. Elder, 2006: A distributed snow-evolution modeling system (SnowModel). *J. Hydrometeor.,* **7,** 1259–1276.

——, R. Pielke Sr., and E. Greene, 1999: Improving first-order snow-related deficiencies in a regional climate model. *J. Geophys. Res.,* **104** (D16), 19 559–19 567.

Livneh, B., Y. Xia, K. Mitchell, M. Ek, and D. Lettenmaier, 2010: Noah LSM snow model diagnostics and enhancements. *J. Hydrometeor.,* **11,** 721–738.

Luce, C., D. Tarboton, and K. Cooley, 1998: The influence of the spatial distribution of snow on basin-averaged snowmelt. *Hydrol. Processes,* **12,** 1671–1683.

Mallat, S., 1989: A theory for multiresolution signal decomposition: The wavelet representation. *IEEE Trans. Pattern Anal. Mach. Intell.,* **11,** 674–693.

Matsui, T., D. Mocko, M.-I. Lee, M. Suarez, and R. Pielke, Sr., 2010: Ten-year climatology of summertime diurnal rainfall rate over the conterminous U.S. *Geophys. Res. Lett.,* **37,** L13807, doi:10.1029/2010GL044139.

Mitchell, K., and Coauthors, 2004: The multi-institution North American Land Data Assimilation System (NLDAS): Utilizing multiple GCIP products and partners in a continental distributed hydrological modeling system. *J. Geophys. Res.,* **109,** D07S90, doi:10.1029/2003JD003823.

Painter, T., K. Rittger, C. McKenzie, P. Slaughter, R. Davis, and J. Dozier, 2009: Retrieval of subpixel snow covered area, grain size, and albedo from MODIS. *Remote Sens. Environ.,* **113,** 868–879, doi:10.1016/J.RSE.2009.01.001.

Quayle, R., D. Easterling, T. Karl, and P. Hughes, 1991: Effects of recent thermometer changes in the cooperative station network. *Bull. Amer. Meteor. Soc.,* **72,** 1718–1723.

Rodell, M., and Coauthors, 2004: The Global Land Data Assimilation System. *Bull. Amer. Meteor. Soc.,* **85,** 381–394.

Rodriguez, E., C. Morris, J. Belz, E. Chapin, J. Martin, W. Daffer, and S. Hensley, 2005: An assessment of the SRTM topographic products. Tech. Rep. JPL D-31639, Jet Propulsion Laboratory, 143 pp.

Saha, S., and Coauthors, 2010: The NCEP Climate Forecast System Reanalysis. *Bull. Amer. Meteor. Soc.,* **91,** 1015–1057.

Salomonson, V., and I. Appel, 2004: Estimating fractional snow coverage from MODIS using the Normalized Difference Snow Index (NDVI). *Remote Sens. Environ.,* **89,** 351–360.

Sellers, P., Y. Mintz, Y. Sud, and A. Dalcher, 1986: A simple biosphere model (SiB) for use within general circulation models. *J. Atmos. Sci.,* **43,** 505–531.

Seyfried, M., and B. Wilcox, 1995: Scale and the nature of spatial variability: Field examples having implications for hydrologic modeling. *Water Resour. Res.,* **31,** 173–184.

Sivapalan, M., and J. Kalma, 1995: Scale problems in hydrology: Contributions of the Robertson workshop. *Hydrol. Processes,* **9,** 243–250.

Stein, U., and P. Alpert, 1993: Factor separation in numerical simulations. *J. Atmos. Sci.,* **50,** 2107–2115.

Tarboton, D. G., T. G. Chowdhury, and T. H. Jackson, 1995: A spatially distributed energy balance snowmelt model. *Biogeochemistry of Seasonally Snow Covered Catchments,* K. A. Tonnessen, M. W. Williams, and M. Tranter, Eds., IAHS Publ. 228, 141–155.

Trujillo, E., J. Ramirez, and K. Elder, 2009: Scaling properties and spatial organization of snow depth fields in sub-alpine forest and alpine tundra. *Hydrol. Processes,* **23,** 1575–1590, doi:10.1002/hyp.7270.

Whiteman, C., 2000: *Mountain Meteorology: Fundamentals and Applications*. Oxford University Press, 355 pp.

Winstral, A., K. Elder, and R. Davis, 2002: Spatial snow modeling of wind-redistributed snow using terrain-based parameters. *J. Hydrometeor.,* **3,** 524–538.

Wood, E., M. Sivapalan, K. Beven, and L. Band, 1988: Effects of spatial variability and scale with implications to hydrologic modeling. *J. Hydrol.,* **102,** 29–47.

——, ——, and ——, 1990: Similarity and scale in catchment storm response. *Rev. Geophys.,* **28,** 1–18, doi:10.1029/RG028i001p00001.

Xia, Y., M. Ek, H. Wei, and J. Meng, 2011: Comparative analysis of relationships between NLDAS-2 forcings and model outputs. *Hydrol. Processes,* **26,** 467–474, doi:10.1002/hyp.8240.

Xie, P., and P. Arkin, 1997: Global precipitation: A 17-year monthly analysis based on gauge observations, satellite estimates, and numerical model outputs. *Bull. Amer. Meteor. Soc.,* **78,** 2539–2558.